Published on 27 March 2014. Downloaded by Pontifícia Universidade Catolica do Rio Grande do Sul on 3/23/2022 6:19:12 PM.

PCCP

PAPER

View Article Online
View Journal | View Issue

TiO_2 nanotubes sensitized with CdSe *via* RF magnetron sputtering for photoelectrochemical applications under visible light irradiation

Cite this: *Phys. Chem. Chem. Phys.*, 2014, **16**, 9148

Jesum A. Fernandes,[a] Pedro Migowski,[b] Zacarias Fabrim,[b] Adriano F. Feil,[c] Guilherme Rosa,[b] Sherdil Khan,[b] Guilherme J. Machado,[b] Paulo F. P. Fichtner,[d] Sérgio R. Teixeira,[b] Marcos J. L. Santos[a] and Jairton Dupont*[a]

Received 23rd January 2014,
Accepted 27th March 2014

DOI: 10.1039/c4cp00361f

www.rsc.org/pccp

Highly ordered TiO_2 NT arrays were easily decorated with CdSe *via* RF magnetron sputtering. After deposition thermal annealing at different temperatures was performed to obtain an improved TiO_2/CdSe interface. The heterostructures were characterized by RBS, SEM, XRD, HRTEM, UV-Vis, EIS, IPCE and current *versus* voltage curves. The sensitized semiconducting electrodes display an enhanced photocurrent density of *ca.* 2 mA cm^{-2} at 0.6 V (*vs.* Ag/AgCl) under visible light ($\lambda > 400$ nm). The sensitized photoelectrodes displayed 3 and 535-fold enhanced photocurrent when compared to bare TiO_2 NTs under 1 sun and under visible light illumination, respectively. IES results confirmed the improved charge transfer across the TiO_2/CdSe/electrolyte interface after annealing at 400 °C. Incident photon-to-electron conversion efficiency measurements confirmed the efficient sensitization by allowing photoresponse in the visible range.

1. Introduction

Due to the growing demand for energy, worldwide research has been focused on the study and development of new and efficient ways to obtain renewable energy. Among all the alternatives, hydrogen is one of the most promising candidates due to its environmentally friendly and renewable aspects.[1,2] Moreover, producing hydrogen using solar irradiation by photoelectrochemical (PEC) water splitting has been attracting large interest since this process can diminish green house gas emission due to the input of light energy.[3–5] Regarding this technology, highly ordered TiO_2 nanotube arrays have been applied as photoanodes in photoelectrochemical cells due to their high chemical stability in aqueous media, associated with large surface area, high conductivity and relatively low production cost.[6,7] Nevertheless, due to the wide band gap (~3.2 for anatase) TiO_2 absorbs only UV light which limits the efficiency for direct solar energy conversion. Different approaches have been explored to improve light absorption of TiO_2, as for instance doping to create donor and acceptor levels within the band gap.[8–11] Another promising way is developing heterostructures, using low band gap sensitizers such as CdSe, CdS and CdTe, which allows for photoexcited electron transfer to the conduction band of TiO_2. These sensitizers are usually obtained by colloidal synthesis, spray pyrolysis and chemical bath deposition.[7,12–17] On the other hand, physical vapour deposition (PVD) techniques are currently widely used in manufacturing of large-scale thin film photovoltaic (PV) devices. Furthermore, the most efficient and lower cost per watt 2nd generation PV cells are produced by PVD techniques such as sputtering deposition.[18–21] Within this context, developing new methodologies can contribute to the understanding of the TiO_2/sensitizer interface and therefore to the development of efficient photoelectrochemical devices. Curiously, the scientific literature lacks reports on the use of sputter deposition of II–VI semiconductors for the TiO_2 sensitization. Thus, considering the high efficiencies obtained in PV technologies and the easy up scaling, one might expect that by using sputtering deposition, highly efficient photoelectrodes can be produced.

In this work, we report the use of radio-frequency (RF) magnetron sputtering to sensitize TiO_2 NTs with CdSe nanoparticles and the study of the influence of CdSe concentration and thermal annealing on the photoelectrochemical and electrical properties of the heterostructures.

2. Experimental

2.1 Synthesis of TiO_2 NTs

TiO_2 NTs were prepared by an anodization process, carried out in a standard two-electrode electrochemical cell with platinum

[a] *Universidade Federal do Rio Grande do Sul, Instituto de Química, PGCIMAT, Av. Bento Goncalves, 9500, P.O.Box 15003, CEP 91501-970, Porto Alegre, RS, Brazil. E-mail: jairton.dupont@ufrgs.br*
[b] *Universidade Federal do Rio Grande do Sul, Instituto de Física, Av. Bento Goncalves, 9500, 91501-970, Porto Alegre, RS, Brazil*
[c] *Pontifícia Universidade Católica do Rio Grande do Sul, Faculdade de Física, Av. Ipiranga, 6681, 90619-900, Porto Alegre, RS, Brazil*
[d] *Universidade Federal do Rio Grande do Sul, Escola de Engenharia, Av. Bento Goncalves, 9500, 91501-970, Porto Alegre, RS, Brazil*

This journal is © the Owner Societies 2014

Published on 27 March 2014. Downloaded by Pontifícia Universidade Católica do Rio Grande do Sul on 3/23/2022 6:19:12 PM.

foil as a counter electrode, under a constant applied voltage of 20 V for 1 h, in an ultrasonic bath. The electrolyte solution was 0.5 wt% NH_4F, 10 wt% H_2O and ethylene glycol. The as-anodized samples were annealed at 400 °C for 3 h at a ramping rate of 5 °C min^{-1} under air.[6,22–24]

2.2 CdSe deposition by RF sputtering

CdSe was deposited on TiO_2 NT substrates, by the technique of RF magnetron sputtering using a compost target of CdSe (99.999%). The background sputtering pressure was 2×10^{-9} mbar and the working pressure was 2×10^{-2} mbar under Ar (99.9999%). A 5 min pre-sputtering was performed to clean the CdSe target before deposition. The sputtering was carried out with an RF power of 50 W and a deposition rate of 0.057 nm s^{-1} at 25 °C, during different periods of 5, 30 and 60 min. After deposition, the samples were annealed at different temperatures of 300 °C, 400 °C and 500 °C under vacuum (2×10^{-7} mbar) for 30 minutes.

2.3 Composition, morphology, optical and structural characterization

Rutherford backscattering spectrometry (RBS) analysis was carried out using a He^{++} ion beam. The detector was positioned at 15° from the beam. Fig. 1a shows the RBS spectrum obtained with a beam energy of 1.4 MeV and Fig. 1b and 4a with a beam energy of 3 MeV. The morphologies of pristine TiO_2 NTs and the heterostructures were characterized by scanning electron microscopy (SEM) in a JEOL 6060. Glancing angle XRD measurements were carried out using a Philips diffractometer with K_α radiation (λ = 1 : 54 Å). All the measurements were performed with a lower incidence angle of 2° and at an angular step of 0.02° for every 20 s intervals within the angular region $2\theta = 20°–50°$. The phases were identified by the software Crystallographica Search Match together with the database ICSD – PDF2-International Centre for Diffraction Data. The samples were investigated by high resolution transmission electron microscopy (HRTEM) using a JEM2010 operated at 200 kV and a TITAN microscope operated at 300 kV. The atomic positions were observed in high-angle annular dark field (HAADF) scanning transmission electron microscopy (STEM) images and energy dispersive X-ray spectroscopy (EDS) line profiles, obtained using a Titan microscope operated at 300 kV. The samples were prepared by dispersing a few milligrams of freestanding CdSe/TiO_2 NTs in acetone at room temperature and drop casting the solution on a 400 mesh carbon-coated Cu grid. UV-vis diffuse reflection was performed using a Varian Cary 5000 UV-Visible spectrophotometer.

2.4 Photoelectrochemical characterization

Photocurrent–voltage (*I–V*) and electrochemical impedance spectroscopy (EIS) experiments were carried out using an Autolab model PGSTAT 100N. The experiments were performed in a quartz cell using standard three-electrode configuration, a platinum wire was used as counter electrode, Ag/AgCl as a reference electrode and a CdSe/TiO_2 NT as a working electrode.

During photocurrent–voltage measurements the working electrode was irradiated with a 300 W Xenon lamp. For polychromatic irradiation the light intensity was calibrated to 100 mW cm^{-2} and either an AM 1.5G filter (1 sun) or a UV cut-off filter (visible light, $\lambda \geq 400$ nm) was used. The electrolyte was 0.24 M Na_2S and 0.35 M Na_2SO_3 aqueous solution, used to prevent photocorrosion of the CdSe.[25,26]

The EIS measurements were performed under dark conditions with a frequency range from 100 kHz to 0.1 Hz and an amplitude of 10 mV under open circuit voltage.[27–29]

Incident photon-to-electron conversion efficiency (IPCE) measurements were performed in a keithley 2400 SourceMeter and a monochromator cornerstone Oriel. A coiled platinum wire in a two electrode cell was used as a counter electrode.[30–32]

3. Results and discussion

In order to isolate the CdSe from the TiO_2 and from impurities related to the anodization process, we have obtained the RBS spectrum of pure CdSe on silicon (Si) substrates (Fig. 1a). One can observe the presence of Si, Cd and Se clearly showing the formation of a highly pure material presenting a 1 : 1 stoichiometry.[33,34] For the CdSe deposited on TiO_2 NTs (Fig. 1b) the 1 : 1 stoichiometry is also observed, however for shorter deposition periods there is a small deficiency of Cd (see Table 1).

The SEM images of the as-deposited samples show that the top tube coverage becomes thicker as the CdSe target is sputtered for longer periods (Fig. 2a). STEM analyses were used to evaluate the CdSe distribution on the outer/inner wall of TiO_2 NTs (Fig. 2b and c). Although CdSe was deposited on all length of the tubes, the highest concentration is localized on

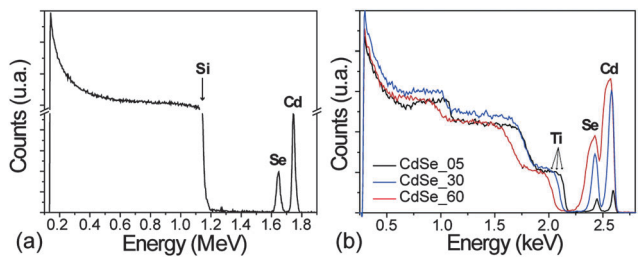

Fig. 1 RBS spectra of CdSe on silicon substrates obtained after 1 minute deposition (a), and CdSe on TiO_2 NTs obtained after 05 min, 30 min and 60 min deposition (b).

Table 1 Characteristics of TiO_2/CdSe photoanodes produced by RF magnetron sputtering

Samples	Deposition time (min)	Annealing (°C)	Concentration ($\times 10^{17}$ at. cm^{-2})		Rate
			Cd	Se	Cd/Se
CdSe_05	05	—	0.54	0.55	0.98
CdSe_30	30	—	3.18	3.21	0.99
CdSe_60	60	—	6.37	6.40	1.00
CdSe_30/300	30	300	2.99	3.03	0.99
CdSe_30/400	30	400	2.90	2.95	0.98
CdSe_30/500	30	500	<LOQ	<LOQ	<LOQ

LOQ: limit of quantification.

Published on 27 March 2014. Downloaded by Pontifícia Universidade Católica do Rio Grande do Sul on 3/23/2022 6:19:12 PM.

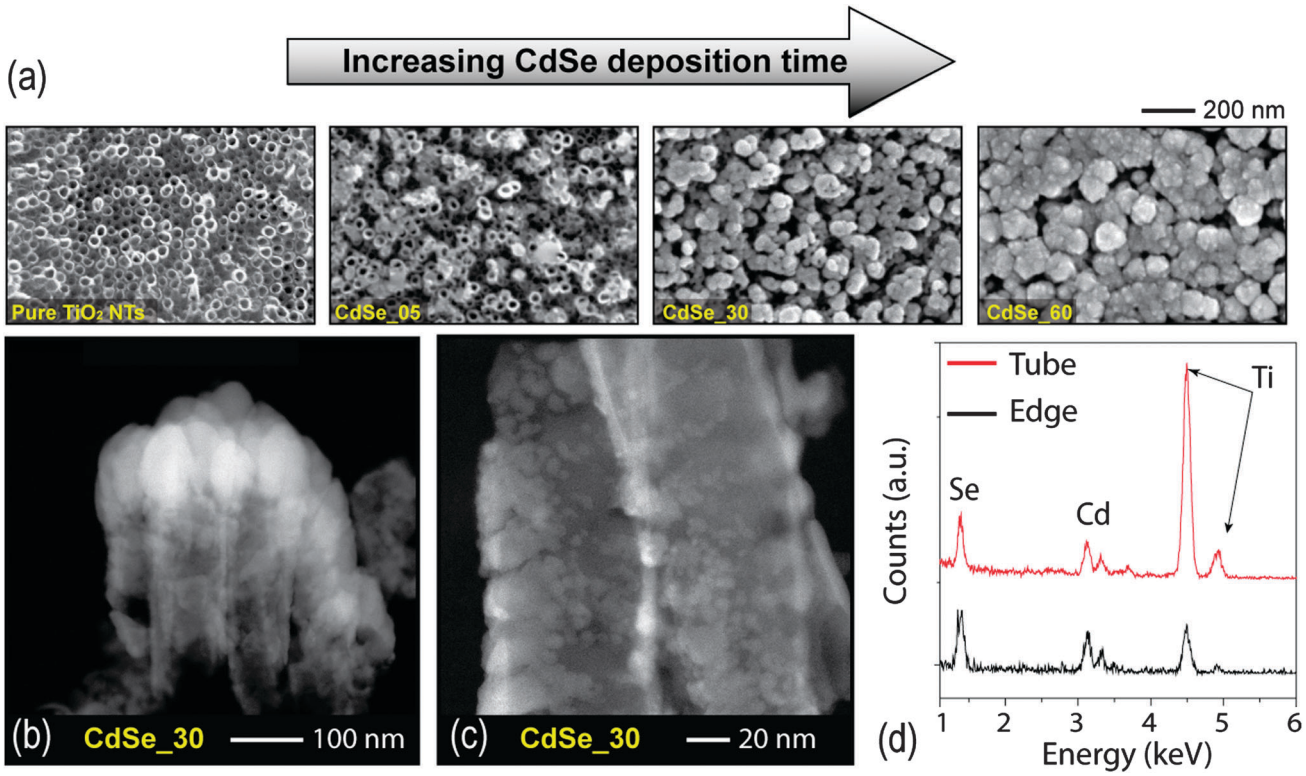

Fig. 2 SEM images of samples obtained with different deposition times (a), STEM images showing CdSe distribution on the TiO_2 NTS for sample CdSe_30 (b and c) and EDS of sample CdSe_30 to confirm the presence of CdSe (d).

the top of the NTs (Fig. 2b). It is possible to observe that CdSe deposition follows the nanotube template without blocking it. This result corroborates the SEM images of CdSe_30. Fig. 2c shows the CdSe cluster distribution on the outer and inner wall of the TiO_2 NTs. In addition, EDS spectra (Fig. 2d) confirm the presence of CdSe on the edge and the centre of the nanotubes. The increase in sputtering time also results in spectral absorption broadening through the visible range (Fig. 3a). The samples obtained after 30 and 60 min of deposition absorb in nearly the entire visible spectrum, meanwhile the sample obtained after 5 minutes presents about the same spectrum as pure TiO_2. The maximum absorbance for CdSe_30 and CdSe_60 is observed at 500 nm and 550 nm, respectively, indicating an increase in average crystal size of CdSe. The absorption band observed for pure TiO_2 from *ca.* 400 to *ca.* 600 nm is characteristic of highly-ordered titania nanotube arrays on titanium foil. Studies on the propagation of electromagnetic waves in the ultraviolet-visible range through these samples have shown that a gradient in the oxide composition from the top of the barrier layer to the Ti metal result in absorption bands in the visible range.[35]

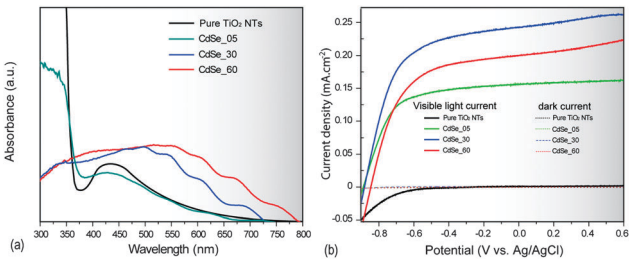

Fig. 3 UV-vis spectra obtained in diffuse reflection mode (a) and photoelectrochemical measurements presented current density–voltage characteristics using visible light irradiation (b).

Current density *versus* potential ($J \times V$) curves, obtained under visible-light, show an interesting relation between optical and photoelectrochemical properties of the TiO_2/CdSe heterostructures (Fig. 3b). The open circuit potential (V_{oc}) of the sensitized samples shifted to more negative potentials, to around −1.0 V *vs.* Ag/AgCl, in relation to the pure TiO_2 sample (V_{oc} of −0.85 V). In addition, all samples showed anodic currents upon illumination, indicating the n-type nature of the semiconductor electrodes. As expected, due to the very low absorptivity under visible irradiation the photocurrent density (J) of pure TiO_2 NTs resembled those exhibited under dark conditions. On the other hand, the CdSe sensitized samples showed PEC response under visible light conditions. Among the sensitized samples, the CdSe_05 which presented the lowest absorbance under visible light, Fig. 3a, also generated the lowest photocurrent Fig. 3b. In addition, the best PEC response was obtained from CdSe_30 and not from CdSe_60, although the last presents the highest absorbance under the visible spectrum.

These results strongly suggest that although increasing CdSe thickness improves optical absorption it also decreases the electron transfer yield from the CdSe sensitizer to the TiO_2.

It is well established that proper annealing can improve particle interaction, thus PEC performance of semiconductor heterostructures.[1,36]

 This journal is © the Owner Societies 2014

Published on 27 March 2014. Downloaded by Pontifícia Universidade Católica do Rio Grande do Sul on 3/23/2022 6:19:12 PM.

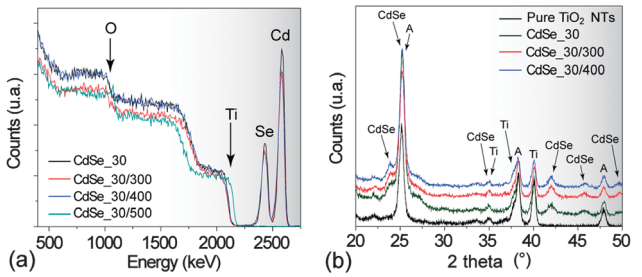

Fig. 4 RBS spectra after annealing (a), structural characterization by XRD (b).

Therefore CdSe_30 samples were annealed at 300, 400 and 500 °C aiming to enhance current density responses. RBS analyses showed that the thermal annealing process does not considerably affect the stoichiometry of the samples, although for the samples CdSe_30/300 and CdSe_30/400 a 6% and 9% loss of CdSe was observed. However, as observed by RBS the CdSe layer vanished completely from the sample CdSe_30/500 (Table 1 and Fig. 4a). Fig. 4b shows the XRD patterns of the samples. The characteristic peak of TiO_2 has been identified at 25.4° which is related to the anatase phase. This peak is observed for all samples, however it broadened when compared to pure TiO_2 due to the overlapping of the CdSe hexagonal phase. The peaks characteristic of CdSe observed at 23.8, 42.1, 45.8 and 49.7° have no interference from the TiO_2 NT substrate. According to SEM and UV-vis analyses before and after annealing the morphology and the optical properties of these samples are not dependent on the thermal treatment. Fig. 5 shows HRTEM images of CdSe crystals covering TiO_2 NTs corroborating with STEM analyses.

The image shows a detailed view of the HRTEM contrast and the distances of the patterns in good agreement with 010 planes of CdSe present in the hexagonal phase, which corroborates the XRD results.

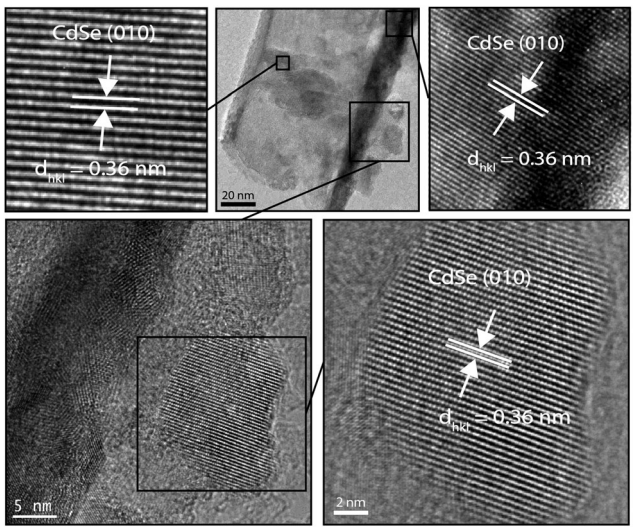

Fig. 5 HRTEM image showing the lattice fringes of CdSe for sample CdSe_30/400.

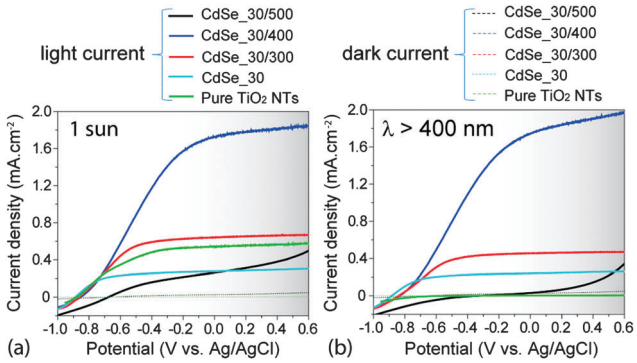

Fig. 6 Current *versus* potential curves of samples with different annealing, measured under 1 sun irradiation (a) and visible light irradiation (b).

In order to evaluate the effect of post deposition thermal treatment on the PEC performance of CdSe_30, $J \times V$ curves were obtained under 1 sun and visible light irradiation, Fig. 6a and b.

Under AM 1.5G conditions, pure TiO_2 NTs present efficiency similar to other systems using the same electrolyte. The worst PEC behaviour was obtained from the sample CdSe_30/500 since the $J \times V$ measurements reveal very low photocurrent in addition to a non-squared curve expected for an efficient system, Fig. 6a. These results were already expected once according to the RBS spectrum, the CdSe was completely removed from the substrate after annealing at 500 °C. Another interesting result is that although sensitized with CdSe, under 1 sun irradiation the CdSe_30/300 generated nearly the same current densities than pure TiO_2 NTs (Fig. 6a). On the other hand, CdSe_30/400 presented a 3-fold enhancement photocurrent when compared to pure TiO_2, at 0.6 V *vs.* Ag/AgCl, resulting in a maximum photocurrent value of $\sim$1.8 mA cm^{-2}. The results obtained under visible light are shown in Fig. 6b. As expected, no photocurrent was generated from pure TiO_2 NTs as they poorly absorb in the visible range. In addition, samples CdSe_30/300 and CdSe_30/400 presented similar photocurrents to those under 1 sun. One can observe a 1.5 and 7 times photocurrent enhancement in samples CdSe_30/300 and CdSe_30/400, respectively, when compared to CdSe_30 (Fig. 6a and b).

These results clearly indicate the existence of an optimum annealing temperature, creating a synergistic interaction between the two materials, improving PEC performance. The improved interaction at the TiO_2/CdSe interface should result in decreased charge transfer resistance and enhanced photocurrent. To elucidate the underlying mechanism of post annealing related to the interface charge transfer, EIS was performed for the samples CdSe_30 and CdSe_30/400. Fig. 7a shows the Nyquist plots obtained for samples CdSe_30 and CdSe_30/400 characteristic of heterogeneous systems. High frequency response represents trapping/detrapping of electrons or electrolyte/counter electrode interface charge transfer. The plots of Fig. 7b represent the cutoff frequency for this charge process which is almost 90 Hz. Similarly, low frequency response conveys the valence band charge transfer resistance at the semiconductor/electrolyte interface.

Published on 27 March 2014. Downloaded by Pontifícia Universidade Católica do Rio Grande do Sul on 3/23/2022 6:19:12 PM.

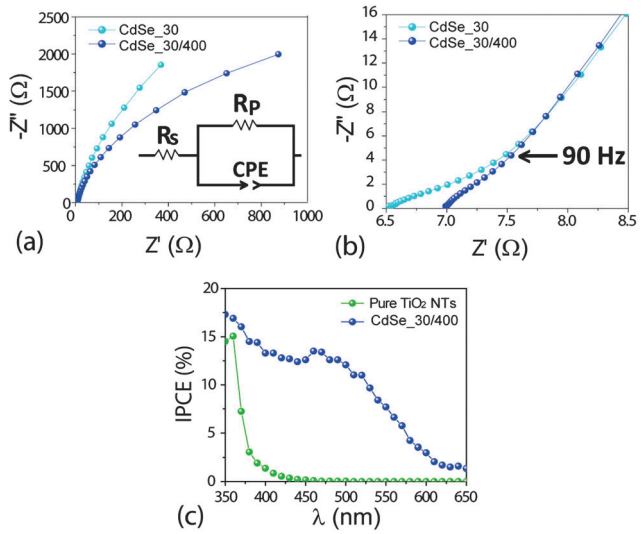

Fig. 7 The EIS measurement to verify the annealing effect on charge transfer (a) shows with details high frequency of samples CdSe_30 and CdSe_30/400 (b), IPCE analyses of the pure TiO_2 NTs and the CdSe sample present highest photocurrent (c).

The arc obtained for CdSe_30/400 clearly indicates low charge transfer resistance when compared to CdSe_30. Considering the Nyquist plots one can observe the existence of only one time constant, resulting from the formation of a CdSe layer deposited by RF magnetron sputtering covering the TiO_2 surface. This result is interesting, once the literature reports two time constants for systems sensitized by chemical routes.[37–39] The total charge transfer resistance at the TiO_2/CdSe interface was calculated by fitting the EIS spectrum considering a series resistance (R_s) with a CPE parallel to resistor (R_p). The series resistance was found to be 7.3 Ω for both samples, which corroborates Fig 7b showing nearly the same resistance at 90 Hz. The parallel resistance was calculated to be 6 kΩ for CdSe_30/400 and 17 kΩ for CdSe_30. Similarly the V_{oc} value under dark for CdSe_30 was measured to be −0.43 V whereas for CdSe_30/400, it was −0.55 V (*vs.* Ag/AgCl) (Table 2). The charge transfer resistance values and the open circuit voltage clearly show that CdSe_30/400 presents improved charge transfer properties when compared to CdSe_30, which corroborates the photocurrent–voltage measurements (Fig. 6a and b).

Fig. 7c shows the IPCE results for pristine TiO_2 nanotubes and for the CdSe_30/400. Pristine TiO_2 presents strong photoresponse in the near-UV region, however a dramatic drop of IPCE is observed for wavelength >370 nm. This result is already expected by considering the large band gap of pure TiO_2.

The sensitized nanotubes (CdSe_30/400) present the ability to harvest and convert light to current in a broad wavelength range, from the near-UV region until around 650 nm. These results are in agreement with the UV-vis spectra (Fig. 3a) showing a match between the optical and the photoelectrochemical behavior of the heterostructure. The IPCE results clearly show that RF magnetron sputtering can be efficiently used to sensitize TiO_2 nanotubes, improving light absorption, in addition to allow photogenerated electrons transfer from the CdSe to TiO_2, increasing IPCE. According to the photoelectrochemical measurements, the main role of CdSe is absorbing visible light and generating excited electrons, while the major role of TiO_2 is allowing charge carrier conduction towards the collecting electrode. This result is interesting, once the literature using either 1 sun[1,7] or visible light[13,14] obtains different results, suggesting that TiO_2 absorption plays an important role in the obtained photocurrent.

Table 2 EIS results of samples as deposited and annealed

Samples	R_s (Ω)	R_p (kΩ)	CPE (μF)	n	V_{oc} (V)
CdSe_30	7.28	17.05	810	0.95	−0.43
CdSe_30/400	7.30	6.01	650	0.96	−0.55

4. Conclusions

In summary, TiO_2 NTs are efficiently sensitized with CdSe using the RF magnetron sputtering technique, resulting in a visible light active heterostructure photoanode. Charge transfer across the TiO_2/CdSe interface as well as photocurrent generation can be improved by controlling annealing temperature. The best photoelectrochemical response was obtained from CdSe_30/400, presenting a photocurrent density of 1.9 mA cm^{-2} at 0.6 V *vs.* Ag/AgCl, resulting in 3 and 535 times enhancement when compared to pure TiO_2 NTs under 1 sun and visible light irradiation. Finally this approach can lead to a more efficient and clean technique to obtain heterostructures for application in different photoelectrochemical devices, including solar cells.

Acknowledgements

The authors thank CNPq, CAPES, GEPSI-PUCRS, Laboratório de Implantação Iônica-UFRGS, Laboratório de Optica-UFRGS, Centro de Microscopia Eletrônica-UFRGS, Laboratório de Conformação Nanométrica-UFRGS and Prof. Dr Daniel L. Baptista for the use of TITAN localized in IMETRO.

Notes and references

1 G. Ai, W. Sun, X. Gao, Y. Zhang and L.-M. Peng, *J. Mater. Chem.*, 2011, **21**, 8749.
2 G. K. Mor, O. K. Varghese, R. H. T. Wilke, S. Sharma, K. Shankar, T. J. Latempa, K.-S. Choi and C. A. Grimes, *Nano Lett.*, 2008, **8**, 1906.
3 A. Fujishima and K. Honda, *Nature*, 1972, **238**, 37.
4 Y. Zhang, Z. Schnepp, J. Cao, S. Ouyang, Y. Li, J. Ye and S. Liu, *Sci. Rep.*, 2013, **3**, 2163.
5 A. Paracchino, V. Laporte, K. Sivula, M. Grätzel and E. Thimsen, *Nat. Mater.*, 2011, **10**, 456.
6 Y. Jun, J. H. Park and M. G. Kang, *Chem. Commun.*, 2012, **48**, 6456.
7 X.-F. Gao, W.-T. Sun, G. Ai and L.-M. Peng, *Appl. Phys. Lett.*, 2010, **96**, 153104.

 This journal is © the Owner Societies 2014

Published on 27 March 2014. Downloaded by Pontifícia Universidade Catolica do Rio Grande do Sul on 3/23/2022 6:19:12 PM.

8 R. Asahi, T. Morikawa, T. Ohwaki, K. Aoki and Y. Taga, *Science*, 2001, **293**, 269.
9 M. Xu, P. Da, H. Wu, D. Zhao and G. Zheng, *Nano Lett.*, 2012, **12**, 1503.
10 J. H. Park, S. Kim and A. J. Bard, *Nano Lett.*, 2005, **6**, 24.
11 S. K. Mohapatra, M. Misra, V. K. Mahajan and K. S. Raja, *J. Phys. Chem. C*, 2007, **111**, 8677.
12 K. Shin, S. i. Seok, S. H. Im and J. H. Park, *Chem. Commun.*, 2010, **46**, 2385.
13 N. Chouhan, C. L. Yeh, S.-F. Hu, R.-S. Liu, W.-S. Chang and K.-H. Chen, *Chem. Commun.*, 2011, **47**, 3493.
14 H. Yang, W. Fan, A. Vaneski, A. S. Susha, W. Y. Teoh and A. L. Rogach, *Adv. Funct. Mater.*, 2012, **22**, 2821.
15 B. Mukherjee, Y. R. Smith and V. Subramanian, *J. Phys. Chem. C*, 2012, **116**, 15175.
16 F. Su, J. Lu, Y. Tian, X. Ma and J. Gong, *Phys. Chem. Chem. Phys.*, 2013, **15**, 12026.
17 B. Mukherjee, W. Wilson and V. Subramanian, *Nanoscale*, 2013, **5**, 269.
18 A. Bosio, A. Romeo, D. Menossi, S. Mazzamuto and N. Romeo, *Cryst. Res. Technol.*, 2011, **46**, 857.
19 I. Repins, M. A. Contreras, B. Egaas, C. DeHart, J. Scharf, C. L. Perkins, B. To and R. Noufi, *Prog. Photovoltaics*, 2008, **16**, 235.
20 T. Wada, N. Kohara, S. Nishiwaki and T. Negami, *Thin Solid Films*, 2001, **387**, 118.
21 N. R. Paudel and Y. Yan, *Thin Solid Films*, 2013, **549**, 30.
22 Y. Alivov, Z. Y. Fan and D. Johnstone, *J. Appl. Phys.*, 2009, **106**, 034314.
23 J. M. Macak, H. Tsuchiya, A. Ghicov, K. Yasuda, R. Hahn, S. Bauer and P. Schmuki, *Curr. Opin. Solid State Mater. Sci.*, 2007, **11**, 3.
24 S. Rani, S. C. Roy, M. Paulose, O. K. Varghese, G. K. Mor, S. Kim, S. Yoriya, T. J. LaTempa and C. A. Grimes, *Phys. Chem. Chem. Phys.*, 2010, **12**, 2780.
25 N. Buehler, K. Meier and J. F. Reber, *J. Phys. Chem.*, 1984, **88**, 3261.
26 J. Hensel, G. Wang, Y. Li and J. Z. Zhang, *Nano Lett.*, 2010, **10**, 478.
27 M.-H. Jung and M. G. Kang, *J. Mater. Chem.*, 2011, **21**, 2694.
28 K. Kim, M.-J. Kim, S.-I. Kim and J.-H. Jang, *Sci. Rep.*, 2013, **3**, 3330.
29 L. Bertoluzzi and J. Bisquert, *J. Phys. Chem. Lett.*, 2012, **3**, 2517.
30 N. Guijarro, T. Lana-Villarreal, I. Mora-Seró, J. Bisquert and R. Gómez, *J. Phys. Chem. C*, 2009, **113**, 4208.
31 J. Yan, Q. Ye and F. Zhou, *RSC Adv.*, 2012, **2**, 3978.
32 J.-H. Yum, E. Baranoff, S. Wenger, M. K. Nazeeruddin and M. Gratzel, *Energy Environ. Sci.*, 2011, **4**, 842.
33 W. K. Chu, J. W. Mayer and M. A. Nicolet, *Backscattering Spectroscopy*, Academic Press, New York, 1978.
34 M. Behar, P. F. P. Fichtner, P. L. Grande and F. C. Zawislak, *Mater. Sci. Eng., R*, 1995, **15**, 1.
35 C. A. Grimes and G. K. Mor, *TiO2 Nanotubes Arrays – Synthesis, Properties and Applications*, Springer, US, 2009.
36 C. F. Chi, S. Y. Liau and Y. L. Lee, *Nanotechnology*, 2010, **21**, 025202.
37 V. Johansson, L. Ellis-Gibbings, T. Clarke, M. Gorlov, G. G. Andersson and L. Kloo, *Phys. Chem. Chem. Phys.*, 2014, **16**, 711.
38 H. Jun, M. Careem and A. Arof, *Nanoscale Res. Lett.*, 2014, **9**, 69.
39 R. S. Mane, D. V. Shinde, S. J. Yoon, S. B. Ambade, J. K. Lee and S.-H. Han, *Appl. Phys. Lett.*, 2012, **101**, 033906.